Available online at www.sciencedirect.com
ScienceDirect
Journal of Power Sources 166 (2007) 450–457
JOURNAL OF POWER SOURCES
www.elsevier.com/locate/jpowsour

Performance of catalysts CuO-ZnO-Al_2O_3, CuO-ZnO-Al_2O_3-Pt-Rh, and Pt-Rh in a small reformer for hydrogen generation

Chih-Yung Huang, Yu-Ming Sun, Chung-Yang Chou, Chin-Chia Su *

Department of Mechanical Engineering, National Taiwan University, No. 1, Sec. 4, Roosevelt Road, Taipei 10617, Taiwan, ROC

Received 15 November 2006; received in revised form 20 December 2006; accepted 20 December 2006
Available online 30 December 2006

Abstract

This study experimentally investigates the performances of catalysts CuO-ZnO-Al_2O_3, CuO-ZnO-Al_2O_3-Pt-Rh, and Pt-Rh in a reformer designed to generate hydrogen from a solution of methanol and water for proton exchange membrane (PEM) fuel cell. The results show that both of the methanol conversion and the hydrogen yield rates increase with temperature. For the three catalysts tested, catalyst CuO-ZnO-Al_2O_3 provides the best performance at temperatures lower than 320 °C. However, at higher temperatures, the performance of this catalyst deteriorates, while that of CuO-ZnO-Al_2O_3-Pt-Rh and Pt-Rh continue to improve. It suggests that the addition of Pt and Rh to the original CuO-ZnO-Al_2O_3 catalyst has a stabilizing effect upon the reforming process under higher temperature conditions. The results also show that a higher methanol feed rate reduces the methanol conversion rate, but increases the hydrogen yield rate. It is found that both of the methanol conversion and the hydrogen yield rates reduce as the steam-to-methanol ratio is increased. Finally, the performance can be significantly improved by introducing a turbulence inducer upstream of the catalyst carrier and by increasing both the length and the cell density of the honeycomb structure.

Keywords: Proton exchange membrane fuel cell; Reformer; Methanol–steam reforming reaction; Catalyst; Conversion rate; Yield rate

1. Introduction

Hydrogen is a highly efficient fuel source for proton exchange membrane (PEM) fuel cells. However, difficulties arise in its storage, filling and transportation. These difficulties can be overcome to a large extent by the in situ generation of hydrogen from other chemicals via a reforming process using appropriate catalysts. Of the various reactants considered for such applications, methanol is regarded as one of the most suitable [1–3].

In general, the design of the reforming system used to generate hydrogen gas is dependent on the specific application for which the hydrogen gas is required. For example, various reforming systems comprising a reformer unit, a catalytic burner and a gas conditioner have been constructed for use in PEM fuel cells designed for automobile applications [4–13]. In [6], Emonts added a catalytic burner to the exit of the nozzle and heat unit to reduce the H_2O, CO_2, CH_3OH and CO contents of the fuel. A compact plate-fin reformer (PFR) has been studied in the literature [14,15]. Edwards et al. [16] built a hot spot methanol processor capable of producing 750 L of hydrogen per hour from a reactor with a volume of 245 cm^3 and a cold start-up time of just 50 s. Reformer units with built-in palladium membranes to provide ultra-pure hydrogen gas were built and tested [10,11,17–21]. Horng [22] investigated the cold start transient characteristics of a small methanol reformer for a fuel cell. Kumar et al. [23] and Ahmed et al. [24] used an ultrasonic nozzle to achieve a rapid mixture for the solution of methanol and water.

In 2002, Holladay et al. [25] presented a novel miniature reformer system for micro fuel cell applications, in which both the reformer and the combustor had a volume of less than 5 mm^3. Subsequently, various study groups proposed alternative mini- and micro-steam reformers characterized by high surface to volume ratios [26–37]. However, these micro reformers generally suffered the disadvantages of high cost and the undesirable ingress of the catalyst powder into the micro-channels of the fuel cell.

Methanol–steam reforming is traditionally performed using CuO-ZnO as a catalyst. However, this catalyst suffers a number of limitations, including poor stability, a restricted life, and a

* Corresponding author. Tel.: +886 2 33662703; fax: +886 2 23631755.
E-mail address: chinchiasu@ntu.edu.tw (C.-C. Su).

0378-7753/$ – see front matter © 2007 Elsevier B.V. All rights reserved.
doi:10.1016/j.jpowsour.2006.12.045

Nomenclature

C	concentration of products (%)
L	length of catalyst carrier (mm)
$\dot{m}$	methanol feed rate (mole min^{-1})
N	honeycomb cell density (cell $in.^{-2}$) (CPSI)
SV	space velocity (h^{-1})
T	temperature of catalytic reaction (°C)
Y	hydrogen yield rate (mole min^{-1})

Greek letters

α	steam-to-methanol ratio (mole $mole^{-1}$)
β	methanol conversion rate (%)

limited high-temperature performance. In [17,38,39], the authors reported that these problems could be resolved to a certain extent via the addition of alumina. Furthermore, Nakamura [40] demonstrated that the addition of a noble metal into the catalyst improved its performance at 400 °C, SV = 5 h^{-1}, and $\alpha = 2$. However, neither amount nor component of the noble metal was mentioned in this work.

Despite the notable contributions of the studies presented above, some points remain to be clarified regarding the optimal reforming system for the generation of hydrogen gas for portable fuel cells via a methanol–steam reforming process. Accordingly, the present study performs a series of experimental investigations to determine the performance of three different catalysts, i.e. CuO-ZnO-Al_2O_3, CuO-ZnO-Al_2O_3-Pt-Rh and Pt-Rh, under various operating conditions and different reformer unit designs. The study shows the catalytic characteristics of Pt and Rh, which were not investigated for the application in the methanol reforming reaction.

2. Experimentation

The performances of CuO-ZnO-Al_2O_3, CuO-ZnO-Al_2O_3-Pt-Rh and Pt-Rh were investigated using the experimental system shown in Fig. 1. The core component of the test system was the reactor unit itself. This unit was made of SCM21 alloy steel and had a length and internal diameter of 145 and 26 mm, respectively. The reactor unit was specifically designed in such a way that it could be easily assembled, dismantled and maintained. Conceptually, the reactor unit could be divided into three separate regions, where each region corresponded to a particular stage of the reforming process. The first region was the turbulence region, located at the entrance of the reactor unit and contained the turbulence inducer shown in Fig. 2. On entering the reactor unit, the reactants were forced to flow within the crosshatched slots machined into the outer rim of the inducer and therefore left the inducer with a high degree of turbulence. The gases then entered the second region of the reactor unit, namely the buffer region, and became thoroughly mixed as a result of turbulence mixing mechanisms. Finally, the mixed gases flowed through the heated catalyst carrier (the third region) and were reformed into hydrogen and various other reaction products.

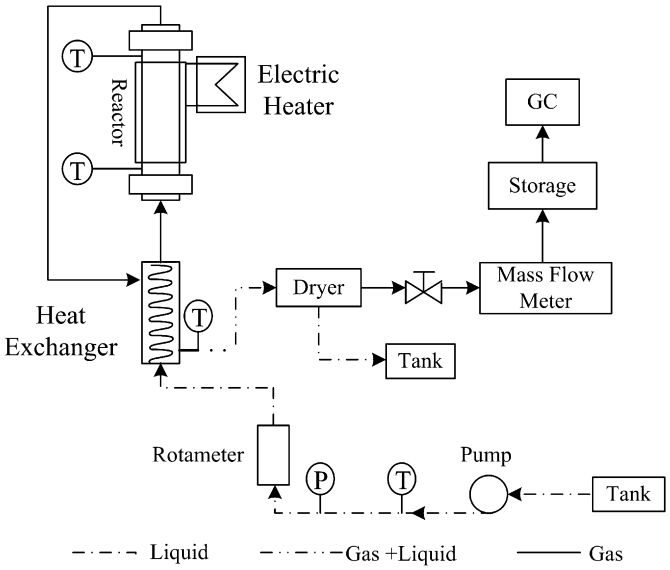

Fig. 1. Schematic illustration of current test system.

As shown in Fig. 3, the catalyst carriers were fabricated with honeycomb structures of different densities. The carriers were manufactured from stainless steel and were designed with a diameter of 23.4 mm such that they would fit tightly within the reactor unit. To investigate the effect of the carrier length on the reaction performance, the carriers were fabricated in two different lengths, i.e. 40 and 65 mm, respectively, such that total carrier lengths of 40, 65, 80 and 105 mm could be obtained by arranging suitable combinations of carriers end-to-end within the reactor unit. The honeycomb structures within the catalyst carriers were constructed with densities of 200, 300 and 400 cells per square inch (CPSI) of cross-sectional area. The surfaces of these cells were coated with a thin layer of the catalyst of interest, i.e. CuO-ZnO-Al_2O_3, CuO-ZnO-Al_2O_3-Pt-Rh or Pt-Rh. The compositional details of these three catalysts are summarized in Table 1. The catalysts were prepared by the impregnation method. The catalyst carrier was, at first, immersed in the aqueous solution of catalyst. Then the carrier was dried in an oven at 105 °C for 24 h and calcined in air in a sintering furnace at 450 °C for 4 h. Finally, aluminum oxide (γ-Al_2O_3) was coated on the carrier to increase the adherence of catalysts. Note that for convenience, the catalysts are denoted simply by A, B and C, respectively. In catalysts A and B, the catalytic effect was produced primarily by the CuO and ZnO components, and the Al_2O_3 component was included mainly to enhance the adherence of the catalyst to the stainless steel surfaces of the honeycomb cells. Catalysts A and B were distinguished by the addition of the noble metals Pt and Rh to the latter. These metals were added to catalyst A to prevent the well-known deterioration in the performance of CuO and ZnO under high-temperature conditions. Catalyst C, containing only the noble metals Pt and Rh, was included in the current experiments simply to investigate the relative effectiveness of different types of catalyst.

As shown in Fig. 1, the test system also included a fuel tank, a pump, a rotameter, a heat exchanger, an electric heater with a power of 550 W, a dryer, a pressure regulator valve, and vari-

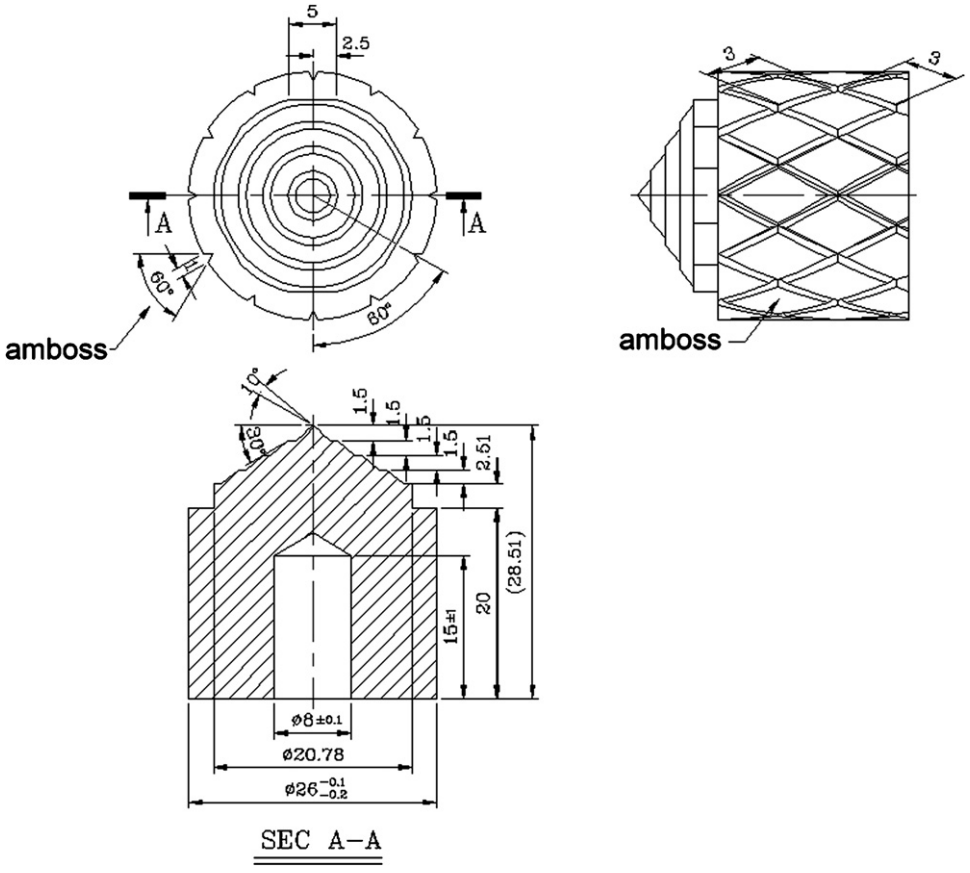

Fig. 2. Design of turbulence inducer.

ous measurement instrumentation. During the experiments, the methanol and water solution was drawn from the fuel tank and pumped through the reactor unit to carry out the reforming process. Note that the mass ratio of the methanol and water in the solution was varied from one experiment to another in order to investigate the effect of the methanol concentration on the reforming reaction. The volumetric flow rate of the solution was monitored by a rotameter, while the temperature and pressure were measured using J-type thermocouples and pressure gauges, respectively.

Since the reforming reaction of methanol and steam is an endothermal process, an electric heater with a power of 550 W was built around the reactor unit to supply the necessary thermal energy and to control the temperature of the reaction process. As a result, the hydrogen and other reaction products leaving the reactor unit had a relatively high temperature. Accordingly, a copper shell-and-coil heat exchanger was installed between the fuel pump and the reactor unit to increase the temperature of the

Fig. 3. Catalyst carriers with different honeycomb cell densities.

Table 1
Details of catalysts

Catalyst	Components	Proportion (%)	Unit mass ($g\,m^{-3}$)
A	CuO	24	424
	ZnO	48	848
	Al_2O_3	28	494
B	CuO	12	212
	ZnO	24	424
	Al_2O_3	14	247
	Pt	37.5	662
	Rh	12.5	221
C	Pt	75	1324
	Rh	25	442

reactants on entering the reactor unit and to decrease the temperature of the products on exiting the reactor unit. On exiting the heat exchanger, the un-reacted methanol and water in a liquid state was separated from the gaseous products by a dryer. The separated liquid solution then flowed under the action of gravity into a separate storage tank, while the gaseous mixture flowed through a mass flow meter incorporating various measurement devices such that not only its mass flow rate, but also its temperature and pressure, could be measured. Finally, the composition of the outlet gas was analyzed using a gas chromatograph (GC) equipped with a thermal conductivity detector.

For the analysis of the test results, the methanol conversion rate, β, is defined as

$$\beta = \left[\frac{\text{Product (CO + CO}_2\text{) (mole min}^{-1}\text{)}}{\text{Feeding MeOH (mole min}^{-1}\text{)}}\right] \times 100\% \quad (1)$$

3. Results and discussions

The experiments performed in the current study were designed to investigate the effect of the following variables on the methanol conversion and hydrogen yield rates during the methanol–steam reforming process: temperature, catalyst type, methanol feed rate, steam-to-methanol ratio, honeycomb cell density, catalyst carrier length, and turbulence.

3.1. Effect of temperature and catalyst type

Fig. 4 shows that for all three catalysts, both of the methanol conversion and hydrogen yield rates increase rapidly as the temperature is increased from 200 to 240 °C. Furthermore, in the temperature range of 200–320 °C the performance of catalyst A is better than that of catalyst B, which in turn is better than that of catalyst C. However, as the temperature is increased from 320 to 360 °C, both of the methanol conversion and hydrogen yield rates produced by catalyst A reduce by approximately 10%. By contrast, the performances of catalysts B and C continue to improve. It is observed that catalyst B provides the best performance of the three catalysts at temperatures higher

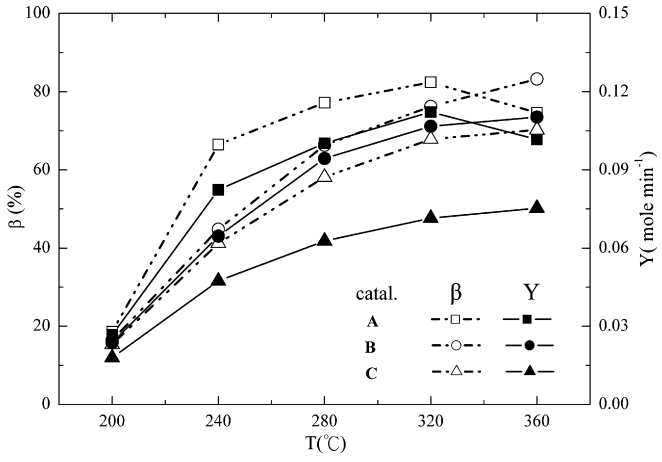

Fig. 4. Variation of conversion and yield rates with temperature (N = 400 CPSI, L = 40 mm, $\dot{m}$ = 0.048 mole min^{-1}, and α = 1.18).

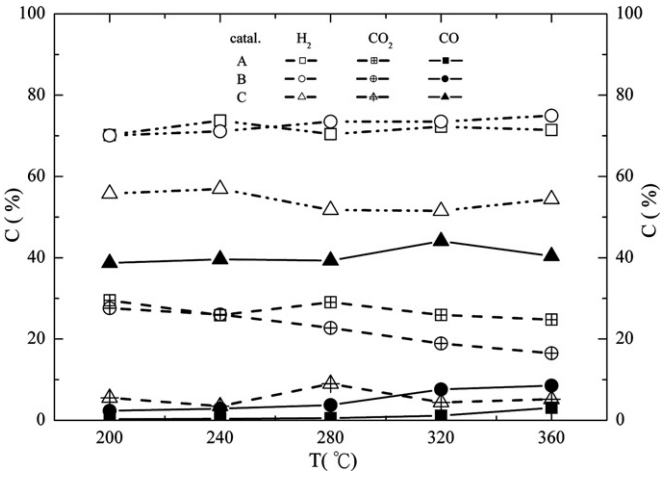

Fig. 5. Variation of product concentration with temperature (N = 400 CPSI, L = 40 mm, $\dot{m}$ = 0.031 mole min^{-1}, and α = 1.18).

than approximately 340 °C. Accordingly, it can be inferred that the addition of the noble metals Pt and Rh to the original catalyst CuO-ZnO-Al_2O_3 successfully prevents the degradation of the performance of CuO and ZnO for the test conditions of N = 400 CPSI, L = 40 mm, $\dot{m}$ = 0.031 mole min^{-1}, T = 320 °C, and α = 1.18. The conversion rate may also be increased through the changes of other parameter, e.g., the length and density of the catalyst carrier and the degree of turbulence, which will be discussed later.

As discussed above, both of the methanol conversion and hydrogen yield rates of catalyst A are higher than those of catalyst B or C at temperatures lower than 320 °C. This result is consistent with the findings reported in [17,38,39], in which the authors conclude that CuO and ZnO dominate the catalytic effect under lower temperature conditions. Referring to Table 1, it can be noticed that the amount of CuO and ZnO in catalyst A are twice those of the corresponding components in catalyst B. However, from Fig. 4, it is observed that the methanol conversion and hydrogen yield rates of catalyst A are not improved by a factor of 2 compared to those of catalyst B. Hence, the enhanced performance of CuO/ZnO-based catalysts does not increase linearly with the amount of CuO and ZnO. The precise nature of the relationship between the CuO and ZnO contents and the performance merits further examination in a future study.

In addition to low conversion and yield rates, catalyst C induced unfavorably high concentration of CO compared with catalyst A or B, as shown in Fig. 5. It can be seen that the concentration of CO induced by catalyst C is approximately 38–44% in the current experimental temperature range. Such a poor performance of catalyst C in inducing high concentration of CO may be explained with the following chemical reactions [41,42]:

$$CH_3OH + H_2O \leftrightarrow CO_2 + 3H_2$$
$$\Delta H_{0,298\,K} = 49.45\,\text{kJ mole}^{-1} \quad (2)$$

$$CH_3OH \leftrightarrow CO + 2H_2 \qquad \Delta H_{0,298\,K} = 90.54\,\text{kJ mole}^{-1} \quad (3)$$

$$CO + H_2O \leftrightarrow CO_2 + H_2 \qquad \Delta H_{0,298\,K} = -41.09\,\text{kJ mole}^{-1} \quad (4)$$

Eq. (2) shows the overall reaction of the methanol–steam reforming process, Eq. (3) represents the methanol decomposition, while Eq. (4) represents the water-gas shift reaction. For the methanol decomposition reaction, it seems that the catalytic effect of the noble metals Pt and Ph is inferior to that of CuO/ZnO combination. Furthermore, the catalytic effect of Pt and Rh on the water-gas shift reaction is also inferior to that of CuO/ZnO combination. Therefore, not only both of the conversion and yield rates induced by the catalysts B and C containing Pt and Rh are lower than those induced by the catalyst A containing neither Pt nor Rh, but also the concentration of CO in the product induced by the former is higher than that by the later. Note that since catalyst B contained less Pt and Rh than catalyst C, the concentration of CO induced by catalyst B is less than that by catalyst C as shown in Fig. 5.

Although high temperature is favorable for the formation of CO by the decomposition of methanol, Fig. 5 shows that at temperature higher than 280 °C, the concentration of CO induced by all of the catalysts increases only slightly, while the amount of CO_2 decrease since Eq. (4) is unfavorable at high temperature. Therefore, in determining the appropriate amount of Pt and Rh added in the catalysts, it is a necessity to strike a compromise between improving the higher temperature performance of the catalysts and limiting the production of CO.

3.2. Catalyst stability

As discussed previously, the performance of catalyst A deteriorates at temperatures above 320 °C. Accordingly, the time-dependent stabilities of the current catalysts were evaluated at a temperature of 320 °C. The stability tests were performed in accordance with the method described in [43,44]. As shown in Fig. 6, the methanol conversion rate of catalyst A was initially higher than that of either catalyst B or C. However, after 1 h, the conversion rate of catalyst A fell below that of catalyst B and finally stabilized after a period of approximately 3 h at a level slightly higher than that of catalyst C. This result suggests that catalyst A is unsuitable for a methanol–steam reforming process conducted under extended high-temperature conditions. In general, the current results for catalyst A are consistent with the findings presented in [45–47], in which it is reported that CuO-ZnO-Al_2O_3 is a suitable catalyst for methanol–steam reforming processes conducted at lower temperatures, i.e. 227–327 °C. The stable conversion rates reported in [47] are 62 and 81% at 220 and 320 °C, respectively. In the present work the stable rate at 320 °C is 74%, which is lower than that reported in [47] at the same temperature. The difference is mainly induced by the content of the catalysts. Fig. 6 shows that the methanol conversion rate of catalyst B remains stable at approximately 87% throughout the 18-h stability test. Accordingly, it appears that the addition of the noble metals Pt and Rh to the original CuO-ZnO-Al_2O_3 catalyst results in a suitable catalyst for steam reforming under protracted high-temperature conditions.

3.3. Effect of methanol feed rate

Fig. 7 plots the variation of the methanol conversion and the hydrogen yield rates with the methanol feed rate as a function of temperature. In general, it is observed that an increasing methanol feed rate causes the methanol conversion rate to decrease, but the hydrogen yield rate to increase.

For a given catalyst carrier, the time spent by the reactants within the reactor unit decreases when the methanol feed rate is increased. Therefore, Eq. (1) implies that the methanol conversion rate will reduce as the methanol feed rate is increased. On the other hand, as shown in Eq. (2) 1 mole of methanol can produce 3 moles of hydrogen. As a result, the hydrogen yield rate increases as the methanol feed rate is increased. The results shown in Fig. 8 may also be discussed in terms of space velocity. For a given catalyst carrier, the space velocity of the mixture increases linearly with methanol flow rate. It can then be inferred that the conversion rate of methanol decreases, while the yield rate of hydrogen increases, with the space velocity.

Fig. 7 shows that the methanol conversion rate is relatively insensitive to changes in the feed rate at either end of the cur-

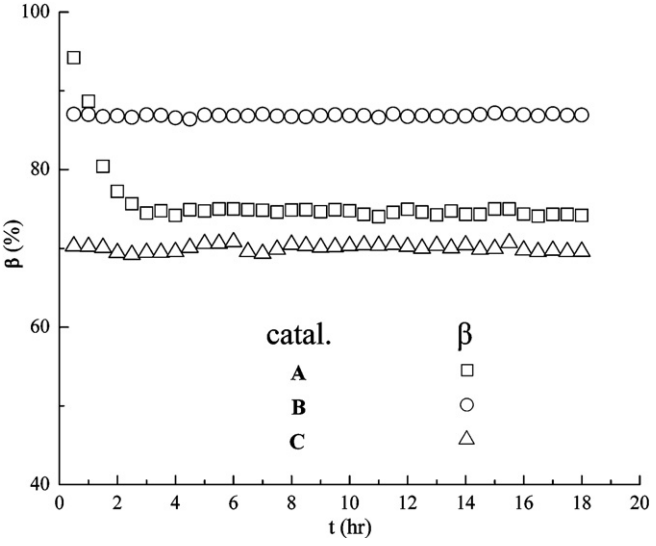

Fig. 6. Stability of catalysts at $T = 320\,^{\circ}C$ ($N = 400$ CPSI, $L = 40$ mm, $\dot{m} = 0.031$ mole min^{-1}, and $\alpha = 1.18$).

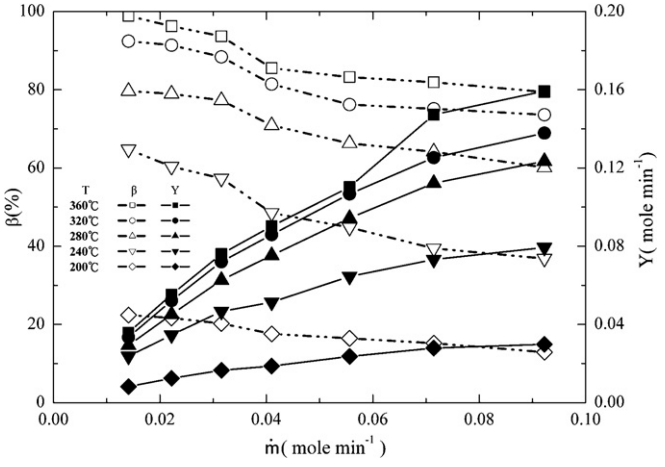

Fig. 7. Variation of conversion and yield rates of catalyst B with methanol feed rate and temperature ($N = 400$ CPSI, $L = 40$ mm, and $\alpha = 1.18$).

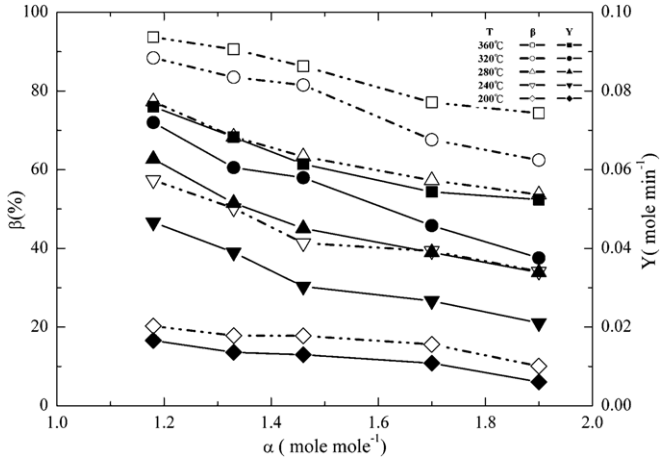

Fig. 8. Variation of conversion and yield rates of catalyst B with steam-to-methanol ratio ($N = 400$ CPSI, $L = 40$ mm, and SV = 20.93 h^{-1}).

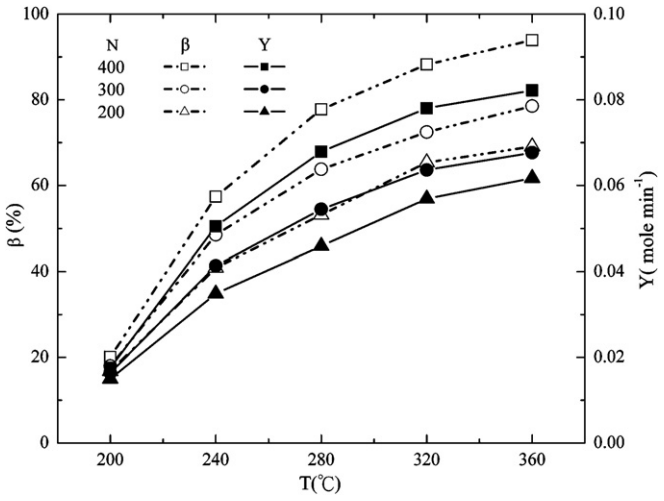

Fig. 9. Variation of conversion and yield rates of catalyst B with temperature and honeycomb cell density ($L = 40$ mm, $\dot{m} = 0.031$ mole min^{-1}, and $\alpha = 1.18$).

rent feed rate range. This implies that attempting to improve the methanol conversion rate by further reducing the methanol feed rate is unlikely to meet with much success. Finally, it is observed that for catalyst B at a temperature of 360 °C, the methanol conversion rate is consistently higher than 80%, irrespective of the methanol feed rate. For a methanol feed rate of less than 0.03 mole min^{-1}, the methanol conversion rate is higher than 93%. Therefore, it is clear that for catalyst B both of the methanol conversion and the hydrogen yield rates are obviously to increase at high temperature.

3.4. Effect of steam-to-methanol ratio

Fig. 8 shows the variation of the methanol conversion and the hydrogen yield rates with the steam-to-methanol ratio as a function of temperature. Note that the results correspond to catalyst B and were obtained under the following conditions: $N = 400$ CPSI, $L = 40$ mm, and SV = 20.93 h^{-1}. It is observed that both of the methanol conversion and the hydrogen yield rates reduce as the steam-to-methanol ratio is increased. Although not shown here, similar trends were observed when testing with catalysts A and C for the same N, L, and SV in the test ranges. Both of reaction rates decrease because the number of moles of methanol reduces as α increases. Consequently, the moles of products CO and H_2 in Eq. (3) also reduce, causing a subsequent reduction in the number of moles of products CO_2 and H_2 in Eq. (4). As shown in Eq. (1), the methanol conversion rate varies in direct proportion to the number of $CO + CO_2$ moles per unit time. Consequently, a reduction in the number of moles of methanol and $CO + CO_2$, leads to a reduction in the methanol conversion and the hydrogen yield rates, respectively. Finally, it can be observed from Fig. 8 that a methanol conversion rate of more than 90% can be obtained by reducing the steam-to-methanol ratio to the values of $\alpha = 1.18$–1.33 and $T = 360$ °C. For $\alpha < 1.18$, the conversion rate may increase further until α is roughly equal to 1.0 as reported in [4]. However, in the range of $1.0 < \alpha < 1.18$, the concentration of CO in the product may rise to an unacceptably high level [4].

3.5. Effects of honeycomb cell density and catalyst carrier length

The reforming reaction of methanol into hydrogen relies on the methanol and steam molecules making sufficient contact with the catalyst to activate the reaction. Therefore, it is reasonable to assume that the performance will vary proportionally with the surface area of the honeycomb structure in the catalyst carrier. Similarly, increasing the length of the honeycomb structure extends the time for which the methanol reactant passes through the catalyst carrier, and hence, intuitively, it is reasonable to expect that the performance will be enhanced.

Fig. 9 shows the variation of the methanol conversion and the hydrogen yield rates with temperature for catalyst carriers with a constant length of 40 mm, but honeycomb densities of 200, 300 and 400 CPSI, respectively. It is observed that both of the conversion and the yield rates increase with temperature and honeycomb density. Since the total internal surface area of the cells in the catalyst carrier with a honeycomb density of 400 CPSI is approximately double that with 200 CPSI, it seems reasonable to assume that the reaction rates observed in the former catalyst carrier will be twice of those observed in the latter. However, the results in Fig. 9 show that this is not in fact the case. This result is reasonable since the amount of catalyst coated on the various carriers was specified as a constant for a given cross-sectional area. Hence, the thickness of the catalyst coated on the cell surfaces of the honeycomb reduced as the number of cells per unit cross-sectional area increased. The results therefore imply a nonlinear relationship between the thickness of the catalyst layer and the reforming rate.

Fig. 10 illustrates the variation of the methanol conversion and the hydrogen yield rates with the carrier length as a function of temperature. Note that the honeycomb density remains constant at 300 CPSI. It can be seen that both of the methanol conversion and the hydrogen yield rates increase significantly as the carrier length is increased from 40 to 65 mm. However, the improvement in the performance becomes gradual as the carrier length is progressively increased to 105 mm. Nonetheless,

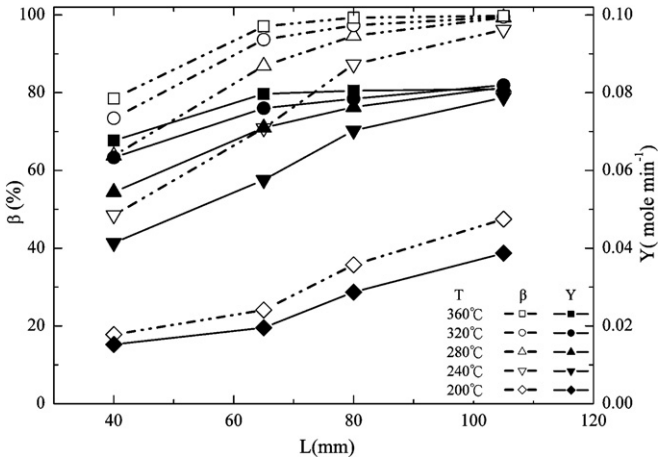

Fig. 10. Variation of conversion and yield rates of catalyst B with honeycomb length ($N = 300$ CPSI, $\dot{m} = 0.031$ mole min^{-1}, and $\alpha = 1.18$).

the results show that using catalyst B (CuO-ZnO-Al_2O_3-Pt-Rh) and specific conditions of $N = 300$ CPSI, $L = 105$ mm, $\alpha = 1.18$, $\dot{m} = 0.031$ mole min^{-1}, and $T = 280$–$360\,^{\circ}$C, yields a methanol conversion rate of nearly 99.9%. Although catalysts B shows excellent stability at $T = 320\,^{\circ}$C as indicated in Fig. 6, such an excellence may require further investigation for even higher temperature.

3.6. Effect of turbulence inducer

Fig. 11 shows the variation of the methanol conversion and the hydrogen yield rates with the methanol feed rate for a reactor unit both with and without a turbulence inducer. When the turbulence inducer is not installed in the reactor unit, the reactants flow primarily through the core region of the reactor unit, and hence the catalyst coated on the cells in the outer region of the honeycomb structure has only a limited effect. Conversely, when the turbulence inducer is introduced upstream of the carrier, the methanol solution flows in the crosshatched slots on the outside surface of the inducer and has a vortex-like flow structure as it enters the honeycomb. From inspection, the results of Fig. 11 indicate that

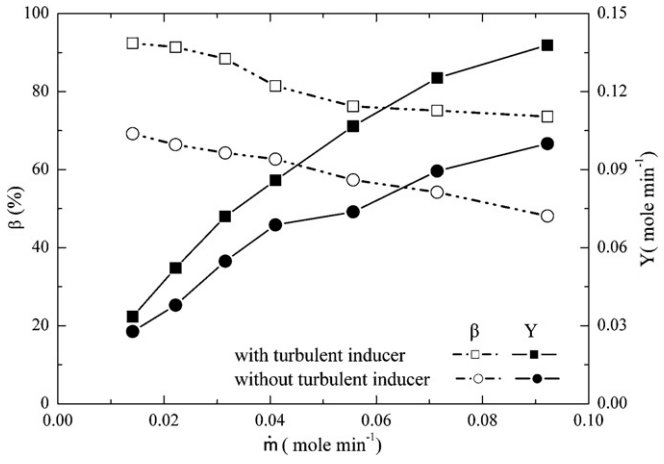

Fig. 11. Effect of turbulence inducer (catalyst B, $N = 400$ CPSI, $L = 40$ mm, $\alpha = 1.18$, and $T = 320\,^{\circ}$C).

the use of the turbulence inducer enhances the methanol conversion rate and the hydrogen yield rate by 33–66 and 20–62%, respectively. The turbulence inducer effectively increases the contact surface area between the reactant gases and the catalyst coated on the honeycomb structure, and hence improves the performance. However, the turbulence inducer in the current test system is intended only to provide a qualitative demonstration of the effect of turbulence on the reforming process, and hence the detailed design of the inducer is not considered. Note that the turbulent flow structure induced by the turbulence generator may shorten the time of contact between the reactants and the catalyst. Consequently, in an extreme case, the presence of the turbulence inducer may actually degrade rather than improve the reaction performance since the time available for reaction within the catalyst carrier is too short. Therefore, optimizing the design of the turbulence inducer may also be a key concern.

4. Conclusion

This study has performed a series of experiments to investigate the catalytic reforming of a methanol solution to generate hydrogen as the fuel source for portable PEM fuel cells, including the catalytic characteristics of Pt and Rh, which was not investigated previously for the application in methanol reforming. Based on the results obtained with various test conditions, the following conclusions can be drawn:

(1) The addition of appropriate amounts of Pt and Rh to the catalyst CuO-ZnO-Al_2O_3 compensates for the reduced performance of CuO and ZnO at high temperatures and ensures that high methanol conversation and hydrogen yield rates can be obtained even at temperatures in excess of 320 °C.
(2) In the stability tests performed at a temperature of 320 °C the methanol conversion rate of catalyst CuO-ZnO-Al_2O_3 falls below that of CuO-ZnO-Al_2O_3-Pt-Rh after a period of 1 h, and then stabilizes after 3 h at a rate slightly higher than that of catalyst Pt-Rh. Conversely, the methanol conversion rate of catalyst CuO-ZnO-Al_2O_3-Pt-Rh remains stable throughout the entire 18 h of the stability test and is generally higher than that of either CuO-ZnO-Al_2O_3 or Pt-Rh. Accordingly, CuO-ZnO-Al_2O_3-Pt-Rh is a suitable catalyst for methanol–steam reforming performed under extended high-temperature conditions.
(3) At temperatures of 320 and 360 °C a low methanol feed rate improves the methanol conversion rate, while a high methanol feed rate improves the hydrogen yield rate. As the methanol feed rate increases, the methanol conversion rate decreases, while the hydrogen yield rate increases.
(4) As the steam-to-methanol ratio is reduced, both of the methanol conversion and the hydrogen yield rates are improved.
(5) The methanol conversion and the hydrogen yield rates both increase with an increasing catalyst carrier length and an increasing honeycomb density.
(6) The use of a turbulence inducer upstream of the catalyst carrier yields a significant improvement in both of the methanol conversion and the hydrogen yield rates.

Acknowledgements

The authors would like to thank LYDS Technology Co. Ltd., Taiwan, for their assistance in preparing the current catalysts. Additionally, the authors gratefully acknowledge the financial support provided to this study by the National Science Council of Taiwan under Grant No. NSC93-2218-E-002-012.

References

[1] S. Ahmed, R. Doshi, R. Kumar, M. Krumpelt, Electr. Hybrid Vehicle Technol. 97 (1997) 77–80.
[2] K.A. Adamson, P. Pearson, J. Power Sources 86 (2000) 548–555.
[3] L.F. Brown, Int. J. Hydrogen Energy 26 (2001) 381–397.
[4] B. HÖhlein, M. Bee, J. BØgild-Hansen, P. BrÖckerhoff, G. Colsnman, B. Emonts, R. Menzer, E. Riedel, J. Power Sources 611 (1996) 43–147.
[5] B. Emonts, J. BØgild-Hansen, S. Loegsgaard-JØrgensen, B. HÖhlein, R. Peters, J. Power Sources 71 (1998) 288–293.
[6] B. Emonts, Catal. Today 47 (1999) 407–414.
[7] W. Wiese, B. Emonts, R. Peters, J. Power Sources 84 (1999) 187–193.
[8] R. Peters, h.G. Düsterwald, B. HÖhlein, J. Power Sources 86 (2000) 507–514.
[9] B. Emonts, J. BØgild-Hansen, H. Schmidt, T. Grube, B. HÖhlein, R. Peters, A. Tschauder, J. Power Sources 86 (2000) 228–236.
[10] J. Han, I.S. Kim, K.S. Choi, J. Power Sources 86 (2000) 223–227.
[11] J. Han, S.M. Lee, H. Chang, J. Power Sources 112 (2002) 484–490.
[12] S. Kawatsu, Proceedings of Fifth Grove Fuel Cell Symposium, London, September, 1997.
[13] J. Hubber, International Automobile Show, Frankfurt, September, 1997.
[14] L. Pan, S. Wang, Int. J. Hydrogen Energy 30 (2005) 973–979.
[15] L. Pan, S. Wang, Chem. Eng. J. 108 (2005) 51–58.
[16] N. Edwards, S. Ellis, J.C. Frost, S.E. Golunski, A.N.J. Van Keulen, N.G. Lindewald, J.G. Reinkingh, J. Power Sources 71 (1998) 123–128.
[17] Y. Lin, M. Rei, Catal. Today 67 (2001) 77–84.
[18] J. Han, I.S. Kim, K.S. Choi, Int. J. Hydrogen Energy 27 (2002) 1043–1047.
[19] R.E. Boxbaum, T.L. Marker, J. Membr. Sci. 85 (1993) 29–38.
[20] C. Nishimura, M. Komaki, M. Amano, Trans. JIM 32 (1991) 501–507.
[21] D.J. Edlund, J. MacCarthy, J. Membr. Sci. 107 (1995) 147–153.
[22] R.F. Horng, Energy Convers. Manage. 46 (2005) 1193–1207.
[23] R. Kumar, S. Ahmed, M. Krumpelt, Electr. Hybrid Vehicle Technol. 96 (1996) 123–127.
[24] S. Ahmed, R. Kumar, M. Krumpelt, US Patent No. 5,942,346 (1996).
[25] J.D. Holladay, E.O. Jones, M. Phelps, J. Hu, J. Power Sources 108 (2002) 21–27.
[26] G.G. Park, D.J. Seo, S.H. Park, Y.G. Yoon, C.S. Kim, W.L. Yoon, Chem. Eng. J. 101 (2004) 87–92.
[27] D.J. Seo, W.L. Yoon, Y.G. Yoon, S.H. Park, G.G. Park, C.S. Kim, Electrochim. Acta 50 (2004) 719–723.
[28] J.D. Holladay, J.S. Waingirh, E.O. Jones, S.R. Gano, J. Power Sources 130 (2004) 111–118.
[29] J.D. Holladay, E.O. Jones, R.A. Dagle, G.G. Xia, C. Cao, Y. Wang, J. Power Sources 131 (2004) 69–72.
[30] C. Horny, L. Kiwi-Minsker, A. Renken, Chem. Eng. J. 101 (2004) 3–9.
[31] P. Reuse, A. Renken, K. Hass-Santo, O. Görke, K. Schubert, Chem. Eng. J. 101 (2004) 133–141.
[32] M.S. Lim, M.R. Kim, J. Noh, S.I. Woo, J. Power Sources 140 (2005) 66–71.
[33] T. Terazaki, M. Nomura, K. Takeyama, O. Nakamura, T. Yamamoto, J. Power Sources 145 (2005) 691–696.
[34] Y. Kawamura, K. Yamamoto, N. Ogura, T. katsumata, A. Igarashi, J. Power Sources 150 (2005) 20–26.
[35] D.W. Matson, P.M. Martin, D.C. Stewart, A.Y. Tonkovich, M. white, J.L. Zilka, G.L. Roberts, Proceedings of the Third International Conference on Microreaction Technology, Berlin, Germany, 2000, p. 62.
[36] J.L. Zilka-Marco, A.Y. Tonkovich, M.J. LaMont, S.P Fitzgerald, D.P VanderWiel, Y. Wang, R.S. Wegeng, Proceedings of the Fourth International Conference on Microreaction Technology, Atlanta, USA, 2000, p. 301.
[37] S.P. Fitzgerald, R.S. Wegeng, A.Y. Tonkovich, Y. Wamg, H.D. Freeman, J.L. Marco, G.L. Roberts, D.P VanderWiel, Proceedings of the Fourth International Conference on Microreaction Technology, Atlanta, USA, 2000, p. 358.
[38] L. Alejo, R. Lago, M.A. Peña, J.L.G. Fierro, Appl. Catal. A 162 (1997) 281–297.
[39] T. Take, T. Yachi, M. Tomura, C. Kiyohara, T. Ishino, H. Kameyama, J. Chem. Eng. Japan 36 (2003) 271–276.
[40] S. Nakamura, Fuel Cell Materials (Update-III), Report No. 5, 2001.
[41] B.A. Pepply, J.C. Amphlett, L.M. Kearns, R.F. Mann, Appl. Catal. A Gen. 179 (1999) 21–29.
[42] S.P. Asprey, B.W. Wojciechowski, B.A. Pepply, Appl. Catal. A Gen. 179 (1999) 51–70.
[43] Y. Teng, H. Sakurai, A. Ueda, T. Kobayashi, Int. J. Hydrogen Energy 24 (1999) 355–358.
[44] I.H. Son, M. Shamsuzzoha, A.M. Lane, J. Catal. 210 (2002) 460–465.
[45] J.C. Amphlett, M.J. Evans, R.A. Jones, R.F. Mann, R.D. Weir, Can. J. Chem. Eng. 59 (1981) 720–727.
[46] J.C. Amphlett, M.J. Evans, R.F. Mann, R.D. Weir, Can. J. Chem. Eng. 63 (1985) 605–611.
[47] C.J. Jiang, D.L. Trimm, M.S. Wainwright, Appl. Catal. A 97 (1993) 145–158.